Surfaces and Interfaces 37 (2023) 102758

Contents lists available at ScienceDirect

Surfaces and Interfaces

journal homepage: www.sciencedirect.com/journal/surfaces-and-interfaces

Deposition of nanocomposites coating on polyimide films by atmospheric pressure plasma for enhanced thermal conductivity

Chengfeng Xiong [a,b,c], Yu Wang [a], Liangliang Lin [d], Ming Gao [a,*], Yifan Huang [a], Paul K Chu [e]

[a] Shenzhen Institute of Advanced Technology, Chinese Academy of Sciences, Shenzhen 518055, China
[b] Suzhou Institute for Advanced Research, University of Science and Technology of China, Suzhou 215123, China
[c] Nano Science and Technology Institute, University of Science and Technology of China, Suzhou 215123, China
[d] School of Chemical and Material Engineering, Jiangnan University, Wuxi 214122, China
[e] Department of Physics, Department of Materials Science and Engineering, and Department of Biomedical Engineering, City University of Hong Kong, Tat Chee Avenue, Kowloon, Hong Kong, China

ARTICLE INFO

Keywords:
Surface modification
Polyimide films
Plasma deposition
Nanocomposite coatings
Thermal conductivity

ABSTRACT

The increasing demand for flexible electronics has spurred the development of flexible substrates with high thermal conductivity. Herein, nanocomposite coatings based on aluminum nitride (AlN) and siloxane matrix are deposited on polyimide (PI) films by atmospheric pressure plasma for improved thermal conductivity. Commercially available aluminum nitride powders are incorporated into methyltrimethoxysilane (MTMS) precursor to form nanocomposite coatings at atmospheric pressure. The evolution of the as-prepared coatings is systematically investigated upon the variations of the deposition time. The smooth surface is transformed into a rough surface with spherical nanoparticles, and the silicon containing functional groups with AlN nanoparticles are introduced into the surface. After 6 min deposition, the surface energies of the PI film can be improved to 32.8 mJ/m^2, and the thermal conductivity can be enhanced to 1.68 W/mK with a coating hardness of 2H. The results demonstrate that the nanocomposite coatings prepared by plasma deposition are an efficient way to modify flexible materials with improved thermal conductivity.

1. Introduction

Polyimide (PI) films are widely used in microelectronics industries due to their good heat resistance and large mechanical strength [1,2]. However, the PI films show surface chemical inertness because of the planar structure and all-aromatic structure. As a consequence, surface modification is usually used to cater to some specific requirements. Various methods have been employed to modify the PI films surfaces including alkali treatment, UV irradiation and plasma treatment [3–5]. As an alternative and eco-friendly approach, direct plasma treatment at atmospheric pressure has been successfully applied to modify the PI film surface. For example, Peng et al. modified PI films using an atmospheric pressure plasma generated by a dielectric barrier discharge (DBD) in argon, and the surface physical and chemical change can be achieved without acid or alkaline usage [6].

With respect to controllable surface modification, different gases have been used to generate different active species in the atmospheric pressure plasma for the treatment of the PI films [7]. Moreover, Abdel–Fattah et al. have used Helium-H_2O plasma to improve the wettability of the PI films surface [8]. However, the plasma-treated films easily lose the generated features as a result of aging with the time progresses [9]. Plasma deposition is one of the desirable techniques to prepare thin coating on the materials surface with long-lasting effects. For polyimide film, Mu et al. prepared SiO_x coating on the film surface by plasma polymer deposition to resist atomic oxygen erosion [10]. This plasma deposition is a very effective method for the modification of the materials surface with functionality.

The development of flexible electronic devices is raising the demand for substrates such as higher voltage and greater power density while maintaining desirable thermal performance. In recent years, surface compounding with thermally conductive layers is an effective way to improve the thermal conductivity of the PI films [11]. Various carbon materials, metals and nitrides have been applied in thermally conductive layers. For example, Tian et al. prepared metal coatings on the surface of polyimide composite using the explosive spraying technology, and the thermal conductivity was achieved to 1.46 W/(m·K) [12]. Guo

* Corresponding author.
E-mail address: ming.gao@siat.ac.cn (M. Gao).

https://doi.org/10.1016/j.surfin.2023.102758
Received 15 November 2022; Received in revised form 13 January 2023; Accepted 17 February 2023
Available online 18 February 2023

et al. prepared graphene oxide/expanded graphite thermally conductive layer on PI composite films [13]. Compared with other thermally conductive materials, aluminum nitride (AlN) has attracted considerable interest because of its high intrinsic thermal conductivity and high breakdown voltage [14]. Moreover, the low cost and simple processability of the AlN are also beneficial for practical application [15]. A common way to prepare AlN coatings on PI film surface is sputtering technology, which use aluminum target and nitrogen ions in vacuum [16,17]. Unfortunately, the complicated vacuum equipment in this configuration is a major bottleneck towards energy and cost saving. Therefore, it is expected to form AlN coating on the PI film surface by a simple strategy at atmospheric pressure condition directly.

It is well known that organic-inorganic hybrid coating can incorporate the inorganic composition into the organic matrix, which is helpful to obtain better comprehensive performance of the coatings, such as abrasive resistance, thermal conductivity and etc. [18,19]. In previous work, siloxane nanocoating has been deposited on glass fibers surface by atmospheric pressure plasma, which provides a solid basis for the extensions of composite coatings [20]. Moreover, the low thermal expansion coefficient of AlN closely matches that of Si [21]. In this study, MTMS/AlN nanocomposite coatings are deposited on PI films by atmospheric pressure plasma. The commercially available aluminum nitride powders are directly incorporated into methyltrimethoxysilane (MTMS) precursor. By regulating the deposition time, the surface physical and chemical changes of the PI films after plasma coatings are investigated systematically, and the surface wetting performance, scratch resistance and the thermal conductivity of the as-prepared coatings are measured.

2. Experimental details

2.1. Materials

Polyimide films (thickness of 0.15 mm; Trademark: Kapton) were supplied by Dupont, USA and the aluminum nitride powder (AlN, ~ 80 nm) was purchased from Kegong Metallurgical Materials Co., Ltd, China. Methyltrimethoxysilane (MTMS, 98%) was obtained from Aladdin, China. All the materials were used as received. Argon (Ar, 99.99%) was supplied by Shenzhen Hongzhou Gas Industry Co., Ltd, China.

2.2. Plasma deposition

The schematic diagram of the preparation process of the nanocomposite coatings is depicted in Fig. 1. The PI films (50 mm × 50 mm) were cleaned ultrasonically with alcohol and deionized water for 15 min and dried at 70 °C for 5 h. 0.1 g/mL of AlN/MTMS was added to a test tube and sonicated for 2 h to form a uniformly mixture. After standing for 1 h, the upper mixture was injected into the plasma together with the carrier gas. The plasma was generated by a customized atmospheric pressure plasma jet (APPJ) powered by a 10 kHz high-voltage power source (Nanjing Suman Electronics Co., Ltd). Ar was employed as both the working and carrier gas and the flow rate was fixed at 3 SLM. Before plasma deposition, the PI films were placed below the plasma jet nozzle, and treated by Ar plasma for 90 s.

2.3. Characterization

The surface morphology was observed by field-emission scanning electron microscopy (SEM, Supra 55, Zeiss, Germany) and the surface roughness was characterized by atomic force microscopy (AFM, Bruker Dimension Icon, Bruker, USA). The surface chemical structure was analyzed by attenuated total reflection (ATR) Fourier transform infrared spectroscopy (FTIR, Nicolet iS50, Thermo Scientific, USA) in the range of 600 - 4000 cm^{-1}. The surface chemical composition was determined by X-ray photoelectron spectroscopy (XPS, ESCALAB 250Xi, Thermo Fisher, USA) using Mg K_{α} radiation and all binding energies were referenced to the C 1s peak.

2.4. Static contact angle measurement

The surface wetting properties were monitored by measuring the static contact angles of water and glycerol (3 μl each droplet) based on the sessile drop technique on the Theta Lite instrument (Biolin Scientific, Sweden). The measurement was repeated 5 times to calculate the averages and standard deviations. The surface energy was estimated by the Owens-Wendt model [22].

2.5. Pencil hardness test

The pencil hardness test was used to assessed the hardness and scratch resistance of the coating according to the GB/T 6739–1996 standard using Pencil Hardness Tester (Dongguan Huaguo Precision Instrument Co., Ltd., China).

2.6. Bending test

The bending durability of the coating was evaluated by a homemade bend tester with a minimum radius of 2 mm ranging from 0 to 135°. After 500 cycles, the surface images of the coatings were monitored using scanning electron microscopy.

2.7. Thermal conductivity measurement

The thermal conductivity was measured on a laser flash apparatus (LFA467, Netzsch, Germany), and an average of three measurements was performed to obtain the results.

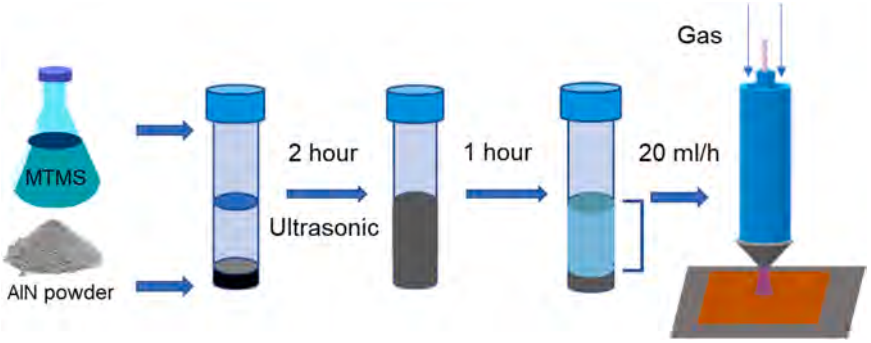

Fig. 1. Schematic illustration of surface modification of the PI films by plasma deposition.

3. Results and discussion

3.1. Surface morphology

Fig. 2 shows the surface morphology of the samples. The control sample exhibits a comparatively smooth surface with flat grooves (Fig. 2a). In comparison, the plasma-deposited samples have a different morphology. The sample deposited for 3 min in Fig. 2b shows spherical nanoparticles about 100 nm in size with good uniformity on the surface. As the deposition time goes up to 6 min (Fig. 2c), the nanoparticles on the surface enlarge in shape and size (about 200 nm). When the time is added to 9 min, the size of the particles increases to 500 nm, and the nanoparticles tend to agglomerate as shown in Fig 2d. The topography varies with the deposited time, mainly due to the excessive generation of the precursor fragments and the aluminum nitride powder. Moreover, compared to the flat surface, the formed nanoparticles have acted as nucleation site, thus facilitating the recombination of the ionized precursors on the particle surface [23].

AFM is used to characterize the surface topography and surface roughness of the samples, and the images are depicted in Fig. 3. The result in Fig. 3a show that the control sample presents small and uniformly distributed protuberances . After plasma deposition for 3 min (Fig. 3b), sharp protuberances appear and the protuberances are evenly distributed. As the deposition time increases to 6 min (Fig 3c), the number of protuberances decreases . When the deposition time reaches 9 min (Fig. 3d), large conical protuberances appear.

The surface roughness (R_a) and root-mean-square roughness (RMS) are used to assess the surface roughness, as shown in Fig. 4. It can be seen that both the Ra roughness and RMS roughness increase with the deposition time increase. After plasma deposition for 9 min, R_a increases to 26.4 nm and RMS increases to 39.1 nm significantly. These results indicate that the topographical features of the surface change gradually with the plasma deposition time.

3.2. Surface chemistry

Fig. 5 shows the ATR-FTIR spectra of the samples revealing peaks related to vibrations of the imide rings (1720 cm^{-1}, 1774 cm^{-1}), aromatic rings (725 cm^{-1}, 820 cm^{-1}, and 1090 cm^{-1}), and the C-N bond (1380cm^{-1}, 1240 cm^{-1}) groups, indicating that the chemical structure of PI film is preserved [24]. All the plasma-deposited samples exhibit a broad band at 1000–1200 cm^{-1} corresponding to Si-O-Si/Si-O-C anti--asymmetric stretching, and the peaks at 1275 cm^{-1} in MA6 and MA9 samples are due to the bending vibration of Si–CH_3 [25,26]. No characteristic peaks are observed from AlN in the coated samples because the hydroxyl groups on the nanoparticles are condensed with MTMS and only the side of the particles away from the AlN particles can be detected by FTIR [27,28].

The chemical states are determined by X-ray photoelectron spectroscopy (XPS). The survey XPS spectrum in Fig. 6a shows the presence of C, O, and Si, and the atomic ratios are listed in Table 1. For the three deposited samples, as the deposition time progresses, the concentration of carbon increases, and the amount of oxygen decreases with the silicon content almost unchanged. Regarding the change in the ratios of O/C and Si/C, both the relative oxygen (O/C) and silicon (Si/C) concentration decreases. This could be explained that after the rise of the deposited time, the excessive AlN powders affect the formation of the Si-O structure. It is worth noting that Al peaks do not appear from the XPS spectra, because XPS is a surface sensitive technique used to analyze the outermost ~10 nm of materials [29]. On the surface of the plasma-deposited sample, the high resolution of Si 2*p* spectra can be deconvoluted into two peaks, locating at 102.7 eV (Si_2O_3) and 103.3 eV (SiO_4), suggesting that MTMS monomer was dissociated by the reaction inside the plasma zone at normal pressure [30].

3.3. Contact angle and surface energy measurement

The wetting behavior of the PI films surface is of great significance to industrial applications. Herein, water and glycerol are used to measure

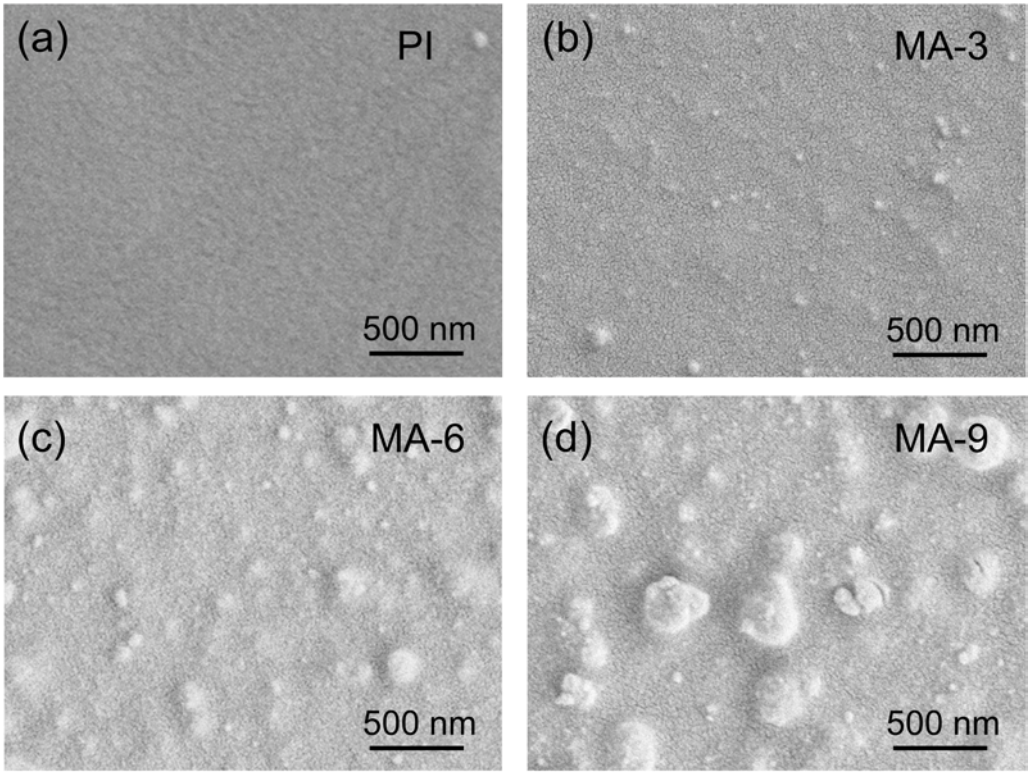

Fig. 2. SEM images of the samples deposited for different time: (a) 0 min, (b) 3 min, (c) 6 min, and (d) 9 min.

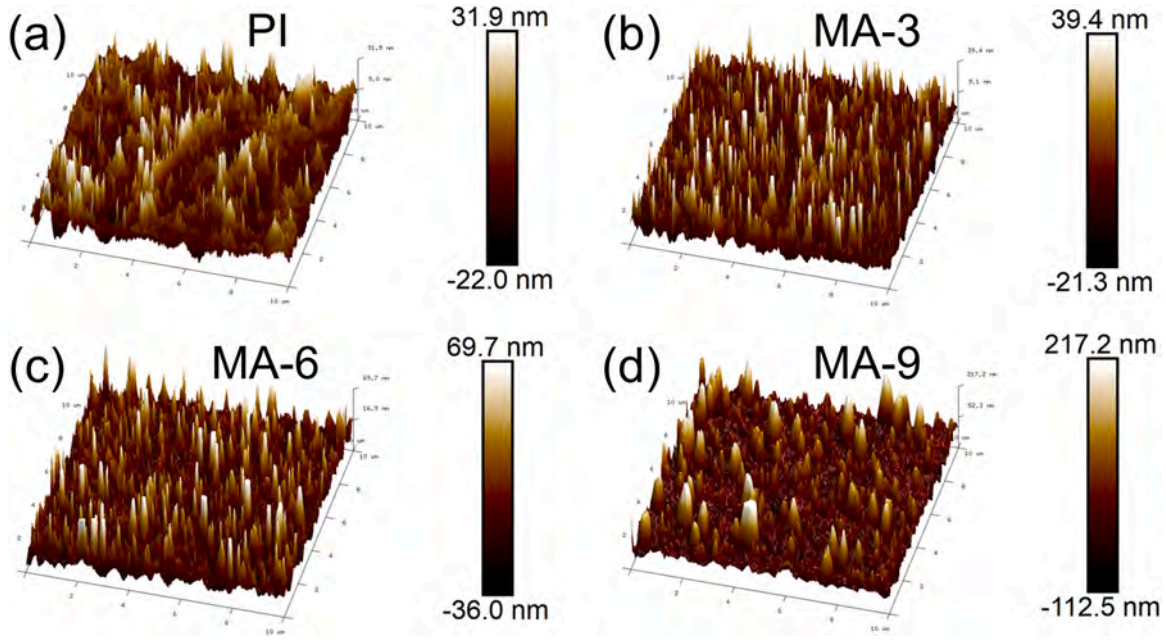

Fig. 3. AFM images of the samples deposited for different time: (a) 0 min, (b) 3 min, (c) 6 min, and (d) 9 min.

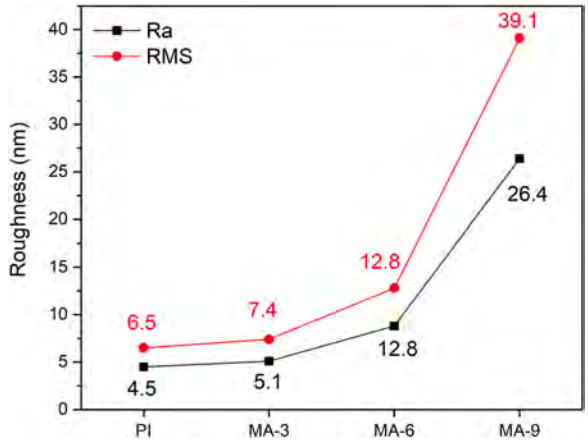

Fig. 4. Surface roughness of the PI film and the samples deposited for 3, 6, and 9 min.

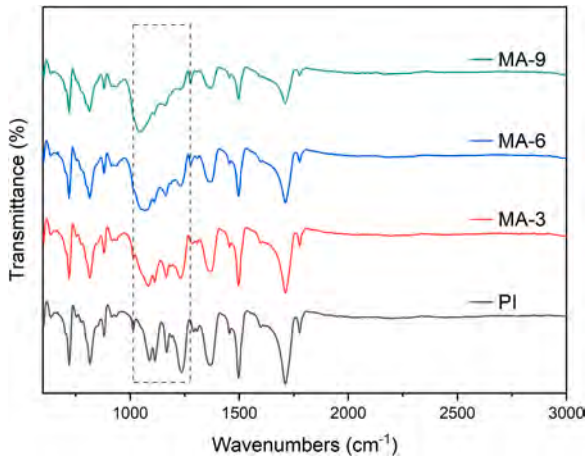

Fig. 5. FTIR spectra of the PI film and the samples deposited for 3, 6, and 9 min.

the static contact angles, and the results are presented in Table 2. The control sample shows contact angles of 78.4° and 75.9° for water and glycerol, respectively. The plasma deposition decreases the contact angles of both liquids due to the surface roughness and surface functional groups. The Owens-Wendt model is an efficient method to derive the surface energy by assuming that the surface free energy is the sum of dispersing (γ^d) and polar (γ^p) components:

$$\gamma = \gamma^d + \gamma^p \quad (1)$$

The surface energy of the polar and disperse components can be calculated by the following equation:

$$\gamma_{LV}\ (1\ +\cos\theta) = 2\sqrt{\gamma^p_{LV} * \gamma^d_{SV}}\ +\ 2\sqrt{\gamma^d_{LV} * \gamma^p_{SV}} \quad (2)$$

where θ is the contact angle, γ^p_{LV} is the polar components of the liquid, γ^d_{LV} is the dispersive components of the liquid, γ^d_{SV} and γ^p_{SV} are the dispersive and polar components of the surface energy of samples. By combing Eqs. (1) and (2), the surface free energies are calculated and depicted in Table 2. The control sample has a surface energy (31.2 mJ/m^2), and the MA-3 and MA-6 samples show a small improved surface energy (32.1 mJ/m^2 and 32.8 mJ/m^2) due to the polar chemical groups. However, the MA-9 sample exhibits a decreased surface energy of 28.7 mJ/m^2. According to the definition of surface energy, the surface energy is determined by the surface excess energy (△G). After the plasma deposition, the oxygen-containing polar groups are introduced to the surface, resulting in the improved surface energy. As the MA-9 sample has the lowest oxygen concentration and the most surface roughness, it exhibits relative inert with a decreased surface energy.

3.4. Scratch resistance and bending test

Scratch resistance is an important parameter to evaluate the durability of the coatings, and pencil hardness test is a simple method widely used for scratch resistance [31]. Pencils with known hardness are prepared according to the standard, and a pencil hardness tester with a load of 750 g holding the pencil at a 45° angle is pushed across the sample surface at a constant speed. The results are shown in Table 3, which discloses that both the MA-3 and MA-6 samples can reach 2H level, while the MA-9 sample show a HB level scratch resistance. This can be attributed to the Si-O-Si structure formed in the organosilicon coatings

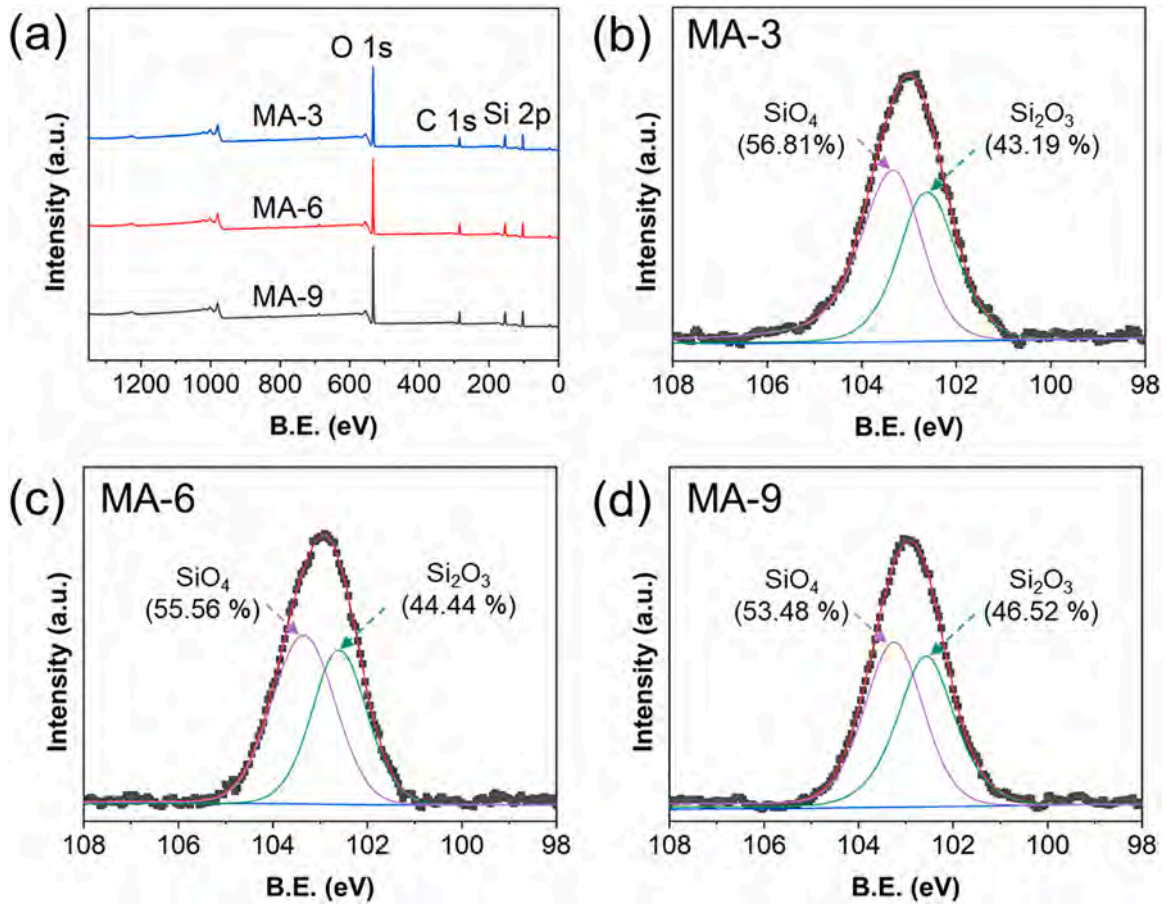

Fig. 6. (a) XPS survey spectra of the samples and Si XPS spectra of the samples deposited for different time: (b) 3 min, (c) 6 min, and (d) 9 min.

Table 1
Relative atomic ratios of the samples.

Samples		MA-3	MA-6	MA-9
Surface relative atomic ratio (%)	**C**	18.74	19.53	21.94
	O	54.34	53.57	51.48
	Si	26.92	26.89	26.58
O/C		2.90	2.74	2.35
Si/C		1.44	1.38	1.21

Table 2
Contact angles and surface energies of the samples.

Samples		PI	MA-3	MA-6	MA-9
Contact angle (°)	**Water**	78.4	71.1	74.2	71.0
	—— Error range	3.2	2.3	0.7	0.6
	Glycerol	75.9	65.5	64.7	73.7
	—— Error range	0.9	3.0	3.0	2.1
Surface energy (mJ/m^2)		31.2	32.1	32.8	28.7

Table 3
Hardness and thermal conductivity of the samples.

Samples	PI	MA-3	MA-6	MA-9
Hardness	——	2H	2H	HB
Thermal Conductivity W/(mK)	0.26	1.37	1.68	1.32
Error range	——	0.11	0.25	0.05

during deposition process, which provides the film surface with excellent mechanical properties [32]. However, when the deposition time reaches 9 min, the large particles and the reduced Si-O-Si structure on the surface results in the scratch resistance of the coatings decreased. As a flexible cover, the coating on the PI films surface need to possess good mechanical flexibility [33]. Fig. 7 depicts the SEM images of the coatings after the flexibility test. All the samples exhibit the surface features similar to those of the initial samples, and there are no surface cracks or defects at the surface of the samples. These images indicate the excellent mechanical flexibility of the coating.

3.5. Thermal conductivity

Owing to the increasing demand for larger power densities in electronic products, more requirements are put forward for the thermal conductivity of materials. As emerging candidates, flexible films with high in-plane thermal conductivity have aroused great interest in the next-generation devices [34]. In this work, the in-plane thermal conductivity is calculated by the following formula:

$$k = \rho \times C_p \times \alpha \tag{3}$$

where k is the thermal conductivity, ρis the density of samples, C_p is the specific heat capacity, and α is the thermal diffusivity of the sample surface. The thermal conductivity is calculated and shown in Table 3. The control PI film has a thermal conductivity of 0.16 W/mK, which is provided by DuPont. Compared to the control sample, all three deposited samples exhibit improved the thermal conductivity, and the highest thermal conductivity can be achieved to 1.68 W/mK for the MA-6 sample, indicating that the introduction of the nanocomposite coating significantly enhances the thermal conductivity of the PI film. As a

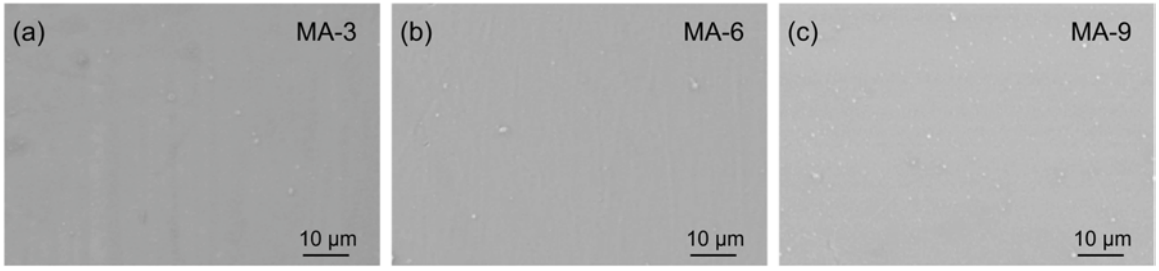

Fig. 7. SEM images of the samples after bending test: (a) 3 min, (b) 6 min and (c) 9 min.

typical insulating dielectric polymer material, the thermal conductivity of the PI film is mostly dominated by phonons [35]. The unique conductive pathways formed by the coatings facilitate the phonon transfer, leading to the enhancement of thermal conductivity. As shown in Table 3, the thermal conductivity of the MA-3 sample is improved to 1.37 W/mK. When the deposition time increases to 6 min, the heat conduction path is more perfect, and the heat could be transferred rapidly through the phonons, resulting in an increased thermal conductivity of 1.68 W/mK. With further extension of the deposition time to 9 min, large particles aggregate on the surface, and the defects may restrict phonon migration, which will impact heat transfer detrimentally and reduce the thermal conductivity to 1.32 W/mK [36].

Fig. 8 shows the formation process of the nanocomposite coating on the PI films surface, which further explains the possible mechanism of enhanced thermal conductivity. As shown in Fig. 8a, when AlN powders are added to the precursor, bonding of hydroxyl groups on the surface of the AlN particles with ionized organosilicon enables the nanoparticles to tightly embed in the Si-O-Si network, resulting in the formation of the composite coatings. The coatings are deposited on the PI films surface, and the network has a bridging effect between AlN and polymer matrix, which can reduce the interfacial thermal resistance [37]. Since phonon transport plays a major contribution in the thermal conductivity, the coatings with interconnected networks act as a highway for phonon transfer. Therefore, the improved thermal conductivity is deduced from to the synergistic effect of the reduced interfacial thermal resistance and the promoted phonon transfer.

4. Conclusion

In summary, atmospheric pressure plasma deposition technique is applied to modify the PI films surface by forming MTMS/AlN nanocomposite coatings. The AlN nanoparticles are well dispersed in the plasma polymerized MTMS matrix, which can endow the coatings with special functionality. The nanocomposite coatings can affect surface morphology, the surface chemical structure, and the surface energy of the PI films. In consideration of the durability of the coatings, the sample deposited for 3 min and 6 min can reach 2H level scratch resistance, while the MA-9 sample show a HB level. The thermal conductivity test shows that all the plasma-deposited samples exhibit the enhanced thermal conductivity, and the best thermal conductivity can be achieved to 1.68 W/mK. The above results indicate that the nanocomposite coatings prepared by plasma deposition could exhibit advanced properties for the surface functional modification of the PI films. This study provides an effective strategy to prepare functional nanocomposite coatings on the surface of flexible materials.

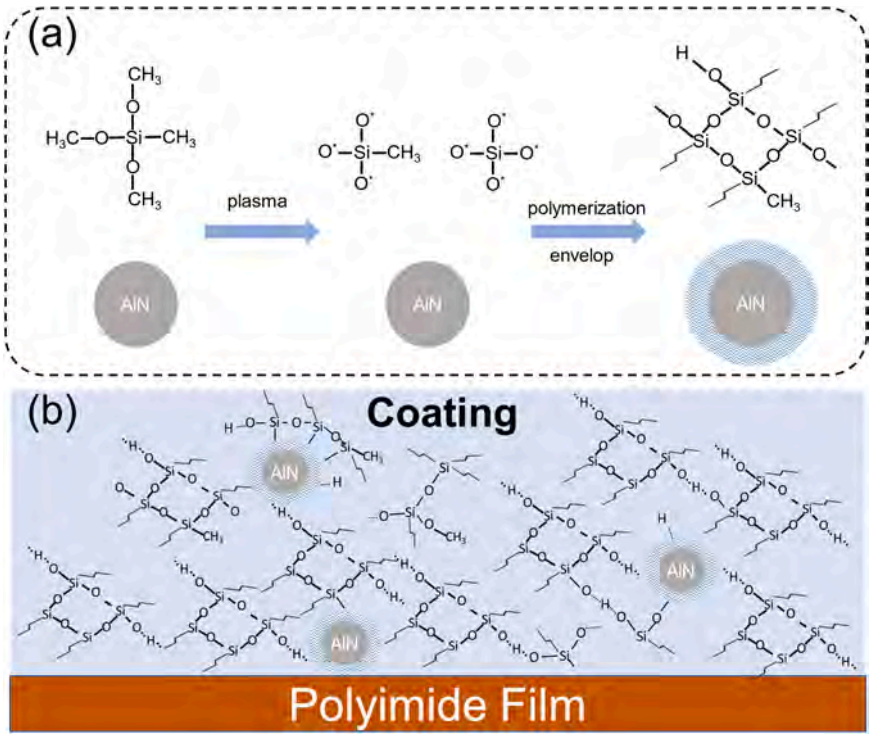

Fig. 8. (a) The possible reaction paths of the nanocomposite coatings prepared by plasma, (b) The nanocomposite coatings on the PI films surface.

CRediT authorship contribution statement

Chengfeng Xiong: Methodology, Investigation, Writing – original draft. **Yu Wang:** Methodology, Investigation, Data curation. **Liangliang Lin:** Visualization, Writing – review & editing. **Ming Gao:** Conceptualization, Methodology, Supervision, Writing – review & editing. **Yifan Huang:** Resources, Supervision. **Paul K Chu:** Resources, Writing – review & editing.

Declaration of Competing Interest

The authors declare that they have no known competing financial interests or personal relationships that could have appeared to influence the work reported in this paper.

Data availability

Data will be made available on request.

Acknowledgments

This work was funded by Shenzhen Science and Technology Innovation Committee (No. JCYJ20180507182200750), Natural Science Foundation of Jiangsu Province (BK20190605), City University of Hong Kong Donation Research Grant (DON-RMG 9229021), City University of Hong Kong Donation Grant (9220061), and Hong Kong ITC (Innovation and Technology Commission) ITF (Innovation and Technology Fund) (GHP/149/20SZ and CityU 9440296). We also thank Prof. Xiaoliang Zeng of Shenzhen Institute of Advanced Electronic Materials.

References

[1] Y. Li, G. Sun, Y. Zhou, G. Liu, J. Wang, S. Han, Progress in low dielectric polyimide film – A review, Prog. Org. Coat. 172 (2022), 107103, https://doi.org/10.1016/j.porgcoat.2022.107103.
[2] P. Ma, C. Dai, H. Wang, Z. Li, H. Liu, W. Li, C. Yang, A review on high temperature resistant polyimide films: heterocyclic structures and nanocomposites, Compos. Commun. 16 (2019) 84–93, https://doi.org/10.1016/j.coco.2019.08.011.
[3] T.J. Liu, C.H. Chen, P.Y. Wu, C.H. Lin, C.M. Chen, Efficient and adhesiveless metallization of flexible polyimide by functional grafting of carboxylic acid groups, Langmuir 35 (2019) 7212–7221, https://doi.org/10.1021/acs.langmuir.9b00354.
[4] R.D. Rusu, C.P. Constantin, M. Drobota, L.M. Gradinaru, M. Butnaru, M. Pislaru, Polyimide films tailored by UV irradiation: surface evaluation and structure-properties relationship, Polym. Degrad. Stab. 177 (2020), 109182, https://doi.org/10.1016/j.polymdegradstab.2020.109182.
[5] A. Grandoni, G. Mannini, A. Glisenti, A. Manariti, G. Galli, Use of statistical design of experiments for surface modification of Kapton films by CF4-O2 microwave plasma treatment, Appl. Surf. Sci. 420 (2017) 579–585, https://doi.org/10.1016/j.apsusc.2017.05.140.
[6] S. Peng L. Li, W. Li, C. Wang, Y. Guo, J. Shi, J. Zhang, Surface modification of polyimide film by dielectric barrier discharge at atmospheric pressure, Plasma Sci. Technol. 18 (2016) 337, https://doi.org/10.1088/1009-0630/18/4/01.
[7] M. Hur, W.S. Kang, J.O. Lee, Y.H. Song, Surface treatment of polyimide substrates using dielectric barrier discharge reactors based on L-shaped electrodes, Plasma Chem. Plasma Process. 35 (2015) 231–246, https://doi.org/10.1007/s11090-014-9598-1.
[8] E. Abdel–Fattah, M. Alshaer, Polyimide surface modification using He-H2O atmospheric pressure plasma jet-discharge power effect, Coatings 10 (2020) 662, https://doi.org/10.3390/coatings10070662.
[9] E. Ortiz-Ortega, S. Hosseini, S.O. Martinez-Chapa, M.J. Madou, Aging of plasma-activated carbon surfaces: challenges and opportunities, Appl. Surf. Sci. 565 (2021), 150362, https://doi.org/10.1016/j.apsusc.2021.150362.
[10] H. Mu, X. Wang, Z. Li, Y. Xie, Y. Gao, H. Liu, Preparation and atomic oxygen erosion resistance of SiOx coating formed on polyimide film by plasma polymer deposition, Vacuum 165 (2019) 7–11, https://doi.org/10.1016/j.vacuum.2019.03.047.
[11] M. Gao, K. Peng, T. Pan, F. Long, Y. Lin, Improving the local thermal conductivity of flexible films by microchannels filled with graphene, Compos. Commun. 25 (2021), 100689, https://doi.org/10.1016/j.coco.2021.100689.
[12] H. Tian, C. Wang, M. Guo, Y. Cui, J. Gao, Z. Tang, Y. Liang, C. Song, H. Wang, G. Jin, S. Wei, Study on process and performance of thermal protective coating on polyimide resin matrix composite, Ceram. Int. 46 (2020) 12744–12758, https://doi.org/10.1016/j.ceramint.2020.02.043.
[13] Y. Guo, H. Qiu, K. Ruan, Y. Zhang, J. Gu, Hierarchically multifunctional polyimide composite films with strongly enhanced thermal conductivity, Nano Micro Lett. 14 (2022) 1–13, https://doi.org/10.1007/s40820-021-00767-4.
[14] T. Matsumae, Y. Kurashima, E. Higurashi, K. Nishizono, T. Amano, H. Takagi, Room temperature bonding of aluminum nitride ceramic and semiconductor substrate, Ceram. Int. 46 (2020) 25956–25963, https://doi.org/10.1016/j.ceramint.2020.07.083.
[15] W.A.L. Sanchez, J.W. Li, H.T. Chiu, C.C. Cheng, K.C. Chiou, T.M. Lee, C.W. Chiu, Highly thermally conductive epoxy composites with AlN/BN hybrid filler as underfill encapsulation material for electronic packaging, Polymers 14 (2022) 2950, https://doi.org/10.3390/polym14142950.
[16] L. Algieri, M.T. Todaro, F. Guido, V. Mastronardi, D. Desmaële, A. Qualtieri, C. Giannini, T. Sibillano, M.D. Vittorio, Flexible piezoelectric energy-harvesting exploiting biocompatible AlN thin films grown onto spin-coated polyimide layers, ACS Appl. Energy Mater. 1 (2018) 5203–5210, https://doi.org/10.1021/acsaem.8b00820.
[17] K. Li, F. Wang, M. Deng, K. Hu, D. Song, Y. Hao, H. Di, K. Dong, S. Yan, Z. Song, K. Zhang, Microstructure and bending piezoelectric characteristics of AlN film for high-frequency flexible SAW devices, J. Mater. Sci. Mater. Electron. 32 (2021) 13146–13155, https://doi.org/10.1007/s10854-021-05830-9.
[18] F. Liu, A. Liu, W. Tao, Y. Yang, Preparation of UV curable organic/inorganic hybrid coatings – a review, Prog. Org. Coat. 145 (2020), 105685, https://doi.org/10.1016/j.porgcoat.2020.105685.
[19] S. Kim, J. Kim, J.H. Kim, Fabrication of insulated metal substrates with organic ceramic composite films for high thermal conductivity, Ceram. Int. 43 (2017) 8294–8299, https://doi.org/10.1016/j.ceramint.2017.03.163.
[20] M. Gao, Y. Wang, Y. Zhang, Y. Li, Y. Tang, Y. Huang, Deposition of thin films on glass fiber fabrics by atmospheric pressure plasma jet, Surf. Coat. Technol. 404 (2020), 126498, https://doi.org/10.1016/j.surfcoat.2020.126498.
[21] Z. Wang, Y. Tong, Y. Wang, Promoting effect of silicon particles on gas-diffusion-reaction system: *in-situ* synthesis of AlN in Al-Si materials, J. Alloy. Compd. 735 (2018) 13–22, https://doi.org/10.1016/j.jallcom.2017.11.108.
[22] A. Liber-Kneć, S. Łagan, Surface testing of dental biomaterials - determination of contact angle and surface free energy, Materials 14 (2021) 2716, https://doi.org/10.3390/ma14112716.
[23] E. Sainz-García, M. López, R. Múgica-Vidal, B. Rojo-Bezares, C. Lozano, A. González-Marcos, P. Toledano, I. Muro-Fraguas, A. Sainz-García, Y. Sáenz, F. Alba-Elías, Promotion of biofilm production via atmospheric-pressure plasma-polymerization for biomedical applications, Appl. Surf. Sci. 581 (2022), 152350, https://doi.org/10.1016/j.apsusc.2021.152350.
[24] Q. Wei, G. Yang, G. Liu, H. Jiang, T. Zhang, Effects and mechanism on Kapton film under ozone exposure in a ground near space simulator, Appl. Surf. Sci 440 (2018) 1083–1090, https://doi.org/10.1016/j.apsusc.2018.01.231.
[25] Y. Li, Z. Li, D. Li, Y. HE, S. Cao, H. Wang, H. Gao, H. Hu, Y. He, Y. Wang, J. Zhu, Roll-to-roll fabrication of large-scale polyorgansiloxane thin film with high flexibility and ultra-efficient atomic oxygen resistance, Plasma Sci. Technol 24 (2022), 065505, https://doi.org/10.1088/2058-6272/ac5f38.
[26] S. Sandeep, A.S. Vishnevskiy, S. Raetz, S. Naumov, D.S. Seregin, A. Husiev, K. A. Vorotilov, V.E. Gusev, M.R. Baklanov, *In-situ* imaging of a light-induced modification process in organo-silica films via time-domain brillouin scattering, Nanomaterials 12 (2022) 1600, https://doi.org/10.3390/nano12091600.
[27] K. Zhang, Y. Lu, N. Hao, S. Nie, Enhanced thermal conductivity of cellulose nanofibril/aluminum nitride hybrid films by surface modification of aluminum nitride, Cellulose 26 (2019) 8669–8683, https://doi.org/10.1007/s10570-019-02694-5.
[28] X. Wang, T. Andritsch, G. Chen, S. Virtanen, The role of the filler surface chemistry on the dielectric and thermal properties of polypropylene aluminum nitride nanocomposites, IEEE Trans. Dielectr. Electr. Insul. 26 (2019) 1009–1017, https://doi.org/10.1109/TDEI.2019.8726006.
[29] L. Lin, L. Rui, Y. Tao, Q. Li, W.H. Chiang, H. Xu, Surface modification of metal substrates using dielectric barrier discharge plasma and the wettability study, J. Taiwan Inst. Chem. E 138 (2022), 104467, https://doi.org/10.1016/j.jtice.2022.104467.
[30] Y.L. Kuo, K.H. Chang, C. Chiu, Carbon-free SiOx ultrathin film using atmospheric pressure plasma jet for enhancing the corrosion resistance of magnesium alloys, Vacuum 146 (2017) 8–10, https://doi.org/10.1016/j.vacuum.2017.09.028.
[31] G. Molero, H.J. Sue, Scratch behavior of model epoxy resins with different crosslinking densities, Mater. Des. 182 (2019), 107965, https://doi.org/10.1016/j.matdes.2019.107965.
[32] J. Ma, J.H. Kim, J. Na, J. Min, G.H. Lee, S. Jo, C.S. Kim, Enhanced polymerization and surface hardness of colloidal siloxane films via electron beam irradiation, ACS Omega 6 (2021) 13384–13390, https://doi.org/10.1021/acsomega.1c01429.
[33] J. Park, C. Kim, J. Lee, H. Kim, Transparent and flexible SiOC films on colorless polyimide substrate for flexible cover window, Micromachines 12 (2021) 233, https://doi.org/10.3390/mi12030233.
[34] C.P. Feng, F. Wei, K.Y. Sun, Y. Wang, H.B. Lan, H.J. Shang, F.Z. Ding, L. Bai, J. Yang, W. Yang, Emerging flexible thermally conductive films: mechanism, fabrication, application, Nano-Micro Lett. 127 (2022) 127, https://doi.org/10.1007/s40820-022-00868-8.
[35] J. Zhou, Y. Wu, H. Kwon, Y. Li, X. Xiao, Y. Ye, Y. Ma, K.E. Goodson, H.Y. Hwang, Y. Cui, Heat conductor-insulator transition in electrochemically controlled hybrid

superlattices, Nano Lett. 22 (2022) 5443–5450, https://doi.org/10.1021/acs.nanolett.2c01407.

[36] F. Zhang, Y. Feng, W. Feng, Three-dimensional interconnected networks for thermally conductive polymer composites: design, preparation, properties, and mechanisms, Mater. Sci. Eng. R 142 (2020), 100580, https://doi.org/10.1016/j.mser.2020.100580.

[37] Q. Ma, Z. Wang, T. Liang, Y. Su, J. Li, Y. Yao, X. Zeng, Y. Pang, M. Han, X. Zeng, J. Xu, L. Ren, R. Sun, Unveiling the role of filler surface energy in enhancing thermal conductivity and mechanical properties of thermal interface materials, Compos. Part A Appl. Sci. 157 (2022), 106904, https://doi.org/10.1016/j.compositesa.2022.106904.